JOURNAL OF GEOPHYSICAL RESEARCH, VOL. 101, NO. C1, PAGES 1163–1181, JANUARY 15, 1996

Modeling the heating and melting of sea ice through light absorption by microalgae

Richard E. Zeebe, Hajo Eicken, Dale H. Robinson, Dieter Wolf-Gladrow, and Gerhard S. Dieckmann

Alfred-Wegener-Institut für Polar- und Meeresforschung, Bremerhaven, Germany

Abstract. In sea ice of polar regions, high concentrations of microalgae are observed during the spring. Algal standing stocks may attain peak values of over 300 mg chl *a* m^{-2} in the congelation ice habitat. As of yet, the effect of additional heating of sea ice through conversion of solar radiation into heat by algae has not been investigated in detail. Local effects such as a decrease in albedo, increasing melt rates, and a decrease of the physical strength of ice sheets may occur. To investigate the effects of microalgae on the thermal regime of sea ice, a time-dependent, one-dimensional thermodynamic model of sea ice was coupled to a bio-optical model. A spectral one-stream model was employed to determine spectral attenuation by snow, sea ice, and microalgae. Beer's law was assumed to hold for every wavelength. Energy absorption was obtained by calculating the divergence of irradiance in every layer of the model ($\Delta z = 1$ cm). Changes in sea ice temperature profiles were calculated by solving the heat conduction equation with a finite difference scheme. Model results indicate that when algal biomass is concentrated at the bottom of congelation ice, melting of ice resulting from the additional conversion of solar radiation into heat may effectively destroy the algal habitat, thereby releasing algal biomass into the water column. An algal layer located in the top of the ice sheet induced a significant increase in sea ice temperature ($\Delta T > 0.3$ K) for snow depths less than 5 cm and algal standing stocks higher than 150 mg chl *a* m^{-2}. Furthermore, under these conditions, brine volume increased by 21% from 181 to 219 parts per thousand, which decreased the physical strength of the ice.

1. Introduction

Sea ice in polar regions provides a variety of habitats for marine microalgae. High biomass has been reported for algal communities located at the surface of the sea ice, within the sea ice as internal bands, within a narrow porous layer located at the bottom of growing sea ice, and within a layer of consolidated ice platelets underlying the sea ice [*Ackley et al.*, 1979; *Horner et al.*, 1992]. In the fast ice of McMurdo Sound (Ross Sea, Antarctica) the bulk of microalgal biomass is typically located within the bottom ice habitat or within the platelet ice layer. For the congelation ice habitat, algal standing stocks of 5 to 600 mg chl *a* m^{-2} have been reported [*Palmisano and Sullivan*, 1983; *SooHoo et al.*, 1987; *Palmisano et al.*, 1988; *Dieckmann et al.*, 1992]. Whereas the composition, growth, and proliferation of sea ice algal communities have been studied in detail (reviewed by *Horner et al.* [1992] and *Legendre et al.* [1992]), their effect on physical processes has received very little attention.

Paper number 95JC02687.
0148-0227/96/95CJ-02687$05.00

Microalgae in sea ice strongly affect the spectral distribution of irradiance and the total irradiance within the ice through light absorption [*Maykut and Grenfell*, 1975; *SooHoo et al.*, 1987; *Arrigo et al.*, 1991, 1993; *Perovich et al.*, 1993]. It has been speculated that algae may also affect the thermal regime of sea ice through conversion of solar radiation into heat [*Cota and Horne*, 1989; *Eicken et al.*, 1991b; *Roesler and Iturriaga*, 1994], thereby affecting the structural stability and melting rate of the sea ice. For example, in McMurdo Sound, *Sullivan et al.* [1983] observed a rapid disintegration of the platelet layer over a 3-4 week period after light penetration at the ice surface was increased by snow clearing, suggesting that ice melting and algal habitat destruction were hastened by absorption of the additional light by microalgae and conversion into heat.

The aim of this paper is to provide a detailed model that calculates the contribution of light absorption and the subsequent release of absorbed energy as heat to the heating and melting of sea ice. In particular, the conditions prerequisite to significant increases in sea ice temperature, brine volume or melting rate were studied for different algal concentrations. We simulated physical and biological conditions that have been reported for both fast ice in McMurdo Sound and the pack ice in the western Weddell Sea.

2. Description of the Model

In order to quantify the influence of microalgae on the heat budget of sea ice, a one-dimensional, thermodynamic model of sea ice [*Maykut and Untersteiner*, 1971] (hereinafter referred to as MU) was coupled to a spectral bio-optical model [*Arrigo et al.*, 1991]. A schematic illustration of the modeled ice cover is presented in Figure 1. New features include a spectrally resolved shortwave flux and equations to determine the brine volume in sea ice. The absorption of light by microalgae is considered by calculating the divergence of irradiance, which represents the connecting link between the thermodynamic model and the bio-optical model (see (9)). Since a fraction of the energy absorbed by the algae is stored as photochemical energy and is not converted into heat, an estimation of the efficiency of photosynthesis is included.

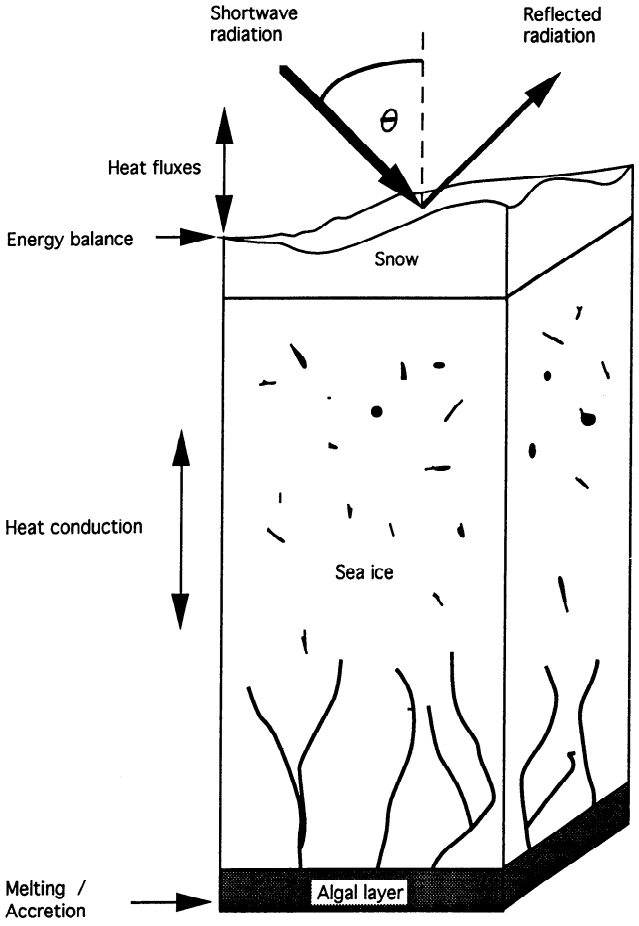

Figure 1. Illustration of the model. Sea ice is viewed as an infinite, horizontally homogeneous slab floating on seawater. The solar shortwave radiation supplies the photosynthetically available radiation that is absorbed by microalgae. The thermodynamic model determines the temperature profile and hence the conductive heat flux through the sea ice. The bio-optical model describes the light attenuation by snow, sea ice, and microalgae.

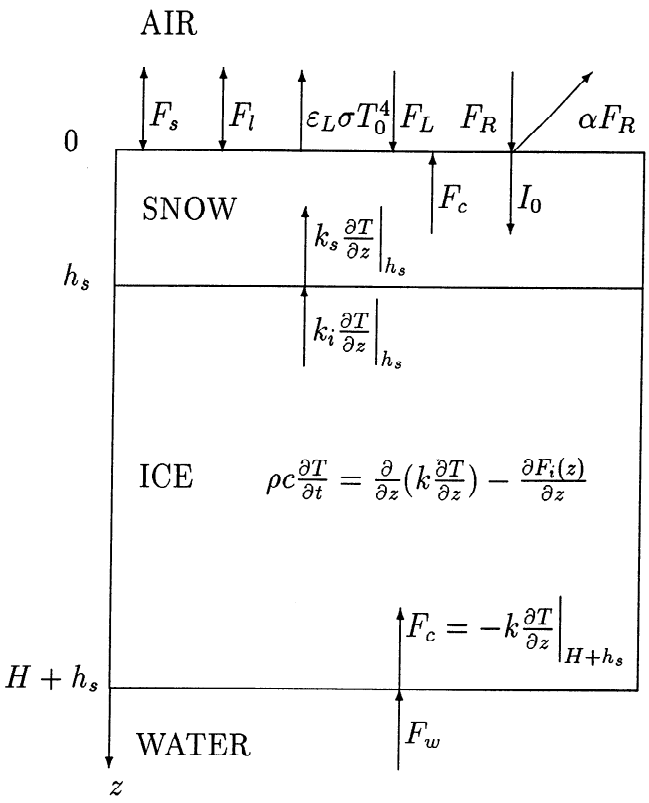

Figure 2. Schematic illustration of the thermodynamic model of sea ice after *Maykut and Untersteiner* [1971]. To determine the surface temperature T_0, the sensible heat flux F_s, latent heat flux F_l, emitted longwave radiation $\varepsilon_L \sigma T_0^4$, incoming longwave radiation F_L, incoming shortwave radiation F_R, and the conductive heat flux F_c must be considered. I_0 denotes the shortwave radiation that penetrates the surface and F_w is the oceanic heat flux. The additional heating through light absorption by microalgae is determined by the calculation of the divergence of irradiance $\partial F_i(z)/\partial z$ in the heat conduction equation.

2.1. The Thermodynamic Model

Only a brief recapitulation of the well-established MU model is presented here. Alterations to this model are described more thoroughly. Sea ice is viewed as an infinite horizontally homogeneous slab floating on seawater. Temperature and thickness of sea ice are controlled by the conduction of heat through the ice slab and the balance of fluxes at its upper and lower surfaces. To solve the heat conduction equation in the interior of the ice, one needs to specify the boundary values of temperature T at the upper surface and at the lower ice-water interface. While the latter equals -1.8°C (freezing point of seawater at a salinity of 34 practical salinity units (psu)), the surface temperature T_0 is obtained by an energy balance at the surface (a flux toward the surface is positive, and a flux away from the surface is negative; see Figure 2). Two possible situations must be considered. If T_0 is below the freezing point, T_0 must be adjusted to balance the fluxes. If, on the other hand, T_0 is at the melting point, ice or snow

will have to melt. Thus the energy balance at the upper surface is described by

$$F_{R,e} + F_L - \varepsilon_L \sigma T_0^4 + F_s + F_l + k\left(\frac{\partial T}{\partial z}\right)\Big|_0 = \begin{cases} 0 & T_0 < 273.15\,K \\ -\rho L \frac{d(H+h_s)}{dt} & T_0 = 273.15\,K \end{cases} \quad (1)$$

where $F_{R,e}$ is the fraction of incoming shortwave radiation that contributes to the surface energy balance (see (2)). F_L is incoming longwave radiation, and $\varepsilon_L \sigma T_0^4$ is emitted longwave radiation, with ε_L denoting the longwave emissivity of the surface material (0.97 for ice and 0.99 for snow); $\sigma = 5.67 \times 10^{-8}$ W m^{-2} K^{-4} is the Stefan-Boltzmann constant. F_s is the sensible heat flux; F_l is the latent heat flux; and $k(\partial T/\partial z)|_0$ is the conductive heat flux at the surface, with z the vertical coordinate and k the thermal conductivity; ρ is the density of the surface layer; L is the latent heat of freezing; H is the ice thickness; and h_s is the thickness of the snow layer (see Figure 2).

Shortwave radiation. The fraction of incoming shortwave radiation that contributes to the energy balance at the surface is calculated as

$$F_{R,e} = \int_{700}^{4000} F_R(\lambda)(1-\alpha_\lambda)d\lambda \quad (2)$$

with spectral incoming shortwave radiation $F_R(\lambda)$ and surface albedo α_λ. Since the absorption of shortwave radiation in sea ice for wavelengths longer than 700 nm is about 3-13 times larger than for wavelengths in the visible range (the extinction coefficient $K_{\lambda,\mathrm{ice}}$ is 1.2 m^{-1} for $\lambda = 460$ nm, while $K_{\lambda,\mathrm{ice}}$ equals 14.1 m^{-1} for $\lambda = 800$ nm [*Grenfell and Maykut*, 1977]), it was assumed that shortwave radiation for wavelengths from 700 to 4000 nm is completely absorbed within the surface layer. Only light in the visible range from 400 to 700 nm was assumed to penetrate into the interior of the ice. This consideration is similar to the assumption of MU, whereby between 17% and 47% of the total net shortwave radiation is penetrating the surface (denoted as I_0). Hence I_0 is the source of the photosynthetically available radiation (PAR) that is absorbed by microalgae and converted into heat. I_0 is calculated as

$$I_0 = \int_{400}^{700} F_R(\lambda)(1-\alpha_\lambda)d\lambda \quad (3)$$

Longwave radiation. The incoming longwave flux F_L is given by

$$F_L = \{1 - 0.261 \exp[-7.77 \times 10^{-4}(273.15 - T_a)^2]\} \times (1 + 0.275\, c_f) \times \sigma T_a^4 \quad (4)$$

where T_a is surface air temperature [*Parkinson and Washington*, 1979]. The cloud cover fraction c_f was taken to be 0.8 in spring and summer for the Weddell Sea [*van Loon*, 1972] and 0.63 in McMurdo Sound [*Schwerdtfeger*, 1970]. Values for T_a have been obtained from data buoys 3313 and 3316 [*Kottmeier and Hartig*, 1990] for the Weddell Sea and from *Schwerdtfeger* [1970] for McMurdo Sound, respectively. In order to eliminate daily fluctuations, which complicate the discussion of the seasonal course of biophysical processes, monthly mean temperatures were interpolated to obtain daily values.

Sensible and latent heat fluxes. Sensible and latent heat fluxes influence the surface temperature of the ice via the surface energy balance (see (1)). During the summertime, sensible and latent heat fluxes typically represent a net loss of heat by the ice, mostly due to the high surface temperature of the ice. Their contribution to the net energy flux at the surface is small (~ -10 W m^{-2}) in comparison to the net shortwave flux (~ 100 W m^{-2}). The sensible heat flux was calculated from the standard bulk aerodynamic formula [e.g., *Cox and Weeks*, 1988]

$$F_s = \rho_a c_a C_s u(T_a - T_0) \quad (5)$$

where $\rho_a = 1.3$ kg m^{-3} is the average air density, $c_a = 1006$ J kg^{-1} K^{-1} is the specific heat of air at constant pressure, $C_s = 0.003$ is the sensible heat transfer coefficient, and u is the wind speed. T_a and T_0 are the surface air temperature and the surface temperature of ice or snow, respectively. The wind speed u was assumed to be 4.4 m s^{-1} in the Weddell Sea [*Kottmeier and Hartig*, 1990] and 5.85 m s^{-1} in McMurdo Sound [*Schwerdtfeger*, 1970].

For the Weddell Sea, latent heat fluxes have been estimated as [*Eicken*, 1992]

$$F_l = 0.25\, F_s. \quad (6)$$

Since this formula may not be applicable to conditions in McMurdo Sound, the latent heat flux for simulations in McMurdo Sound was calculated according to [*Maykut*, 1978]

$$F_l = 0.622 \rho_a L_s C_l u(f_h e_{sa} - e_{s0})/p_0 \quad (7)$$

where e_{sa} and e_{s0} are the vapor pressure of the air at the height of the measurement (usually about 10 m above the surface) and at the surface, respectively. The air at the surface is assumed to be at saturation [*Maykut*, 1978]. $L_s = 2.834 \times 10^6$ J kg^{-1} is the latent heat of vaporization, $C_l = 1.37 \times 10^{-3}$ is the latent heat transfer coefficient, and $p_0 = 986.2$ mbar is the mean air pressure in McMurdo Sound from October to January [*Schwerdtfeger*, 1970]. Since no field data were available for the relative humidity f_h in McMurdo Sound, f_h was set at a value of 80%, which is typical for these Antarctic regions [e.g., *König-Langlo*, 1992]. The sensitivity of the model to this parameter is examined in section 3.3. The vapor pressure e_s was determined from an empirical formula [*Parkinson and Washington*, 1979]

$$e_s = 610.7 \times 10^{9.5[(T-273.15)/(T-7.66)]} \quad (8)$$

Heat conduction. The transfer of heat in the ice

Table 1. Coefficients for the Functions $F_1(T)$ and $F_2(T)$

T, °C	α_0	α_1	α_2	α_3
		$F_1(T)$		
$0 > T > -2$	-4.1221×10^{-2}	-1.8407×10^{1}	5.8402×10^{-1}	2.1454×10^{-1}
$-2 \geq T > -22.9$	-4.723	-2.245×10^{1}	-6.397×10^{-1}	-1.074×10^{-2}
		$F_2(T)$		
$0 > T > -2$	9.0312×10^{-2}	-1.6111×10^{-2}	1.2291×10^{-4}	1.3603×10^{-4}
$-2 \geq T > -22.9$	8.903×10^{-2}	-1.763×10^{-2}	-5.330×10^{-4}	-8.801×10^{-6}

T is temperature. Coefficients α_i are given by *Leppäranta and Manninen* [1988] for the temperature range from −2°C to 0°C and by *Cox and Weeks* [1983] from −22°C to −2°C.

and snow is described by

$$\rho c \frac{\partial T}{\partial t} = \frac{\partial}{\partial z}(k \frac{\partial T}{\partial z}) - \frac{\partial F_i(z)}{\partial z} \quad (9)$$

where ρ is the density, c is the specific heat, and k is the thermal conductivity of sea ice or snow, $\partial F_i(z)/\partial z$ is the divergence of irradiance, T is the temperature at depth z, and t refers to time. Strictly speaking, $\partial F_i(z)/\partial z$ is the heat flux generated by the absorption of irradiance (since the storage of photosynthetic energy is taken into account; see (17)) but is called the divergence of irradiance for simplicity. The density ρ and the thermal conductivity k of sea ice were determined from *Cox and Weeks* [1983, 1988]

$$\rho = (1 - V_a)\frac{\rho_i F_1}{F_1 - \rho_i S F_2} \quad (10)$$

$$k = (1 - V_a - V_b)k_i + V_b k_b \quad (11)$$

with

$$V_b = \frac{\rho S}{F_1} \quad (12)$$

where $V_a = 15$ parts per thousand (ppt) is the gas volume and V_b is the brine volume, ρ_i is the density of pure ice (917 kg m^{-3}), and S is the sea ice salinity. The thermal conductivity of pure ice k_i and pure brine k_b are obtained from *Cox and Weeks* [1988]

$$k_i = 418.6[5.35 \times 10^{-3} - 2.568 \times 10^{-5}(T - 273.15)] \quad (13)$$

$$k_b = 418.6[1.25 \times 10^{-3} + 3.0 \times 10^{-5}(T - 273.15)] \quad (14)$$

The empirical functions F_1 and F_2 are least squares curves of the form [*Cox and Weeks*, 1983]

$$F(T) = \alpha_0 + \alpha_1 T + \alpha_2 T^2 + \alpha_3 T^3 \quad (15)$$

The coefficients α_i are given by *Leppäranta and Manninen* [1988] for the temperature range from −2°C to 0°C and by *Cox and Weeks* [1983] for the temperature range from −22°C to −2°C (Table 1). The specific heat c was calculated as [*Schwerdtfeger*, 1963]

$$c = c_i - \frac{S(c_w - c_i)}{\alpha(T - 273.15)} + \frac{SL_i}{\alpha(T - 273.15)^2} \quad (16)$$

with $c_i = 2.01 \times 10^3$ J kg^{-1} K^{-1} the specific heat of pure ice, $c_w = 4.23 \times 10^3$ J kg^{-1} K^{-1} the specific heat of water, $L_i = 333.4 \times 10^3$ J kg^{-1} the latent heat of pure ice, and $\alpha = 18.2$ K^{-1} the constant describing the linear relationship between the temperature and the salinity of the brine. As the thermal properties ρ, k, and c of sea ice vary with temperature and salinity, they are calculated in every layer of the model, depending on the current temperature and salinity profile. The salinity profiles (Figure 3) for the Weddell Sea and McMurdo Sound were obtained by least squares curves using field data from *Eicken et al.* [1991a] and from G. Dieckmann (unpublished data, 1989), respectively. The smoothed salinity profiles (Figure 3) were used to eliminate salinity fluctuations on small scales, which result in discontinuous brine volume profiles and complicate the dis-

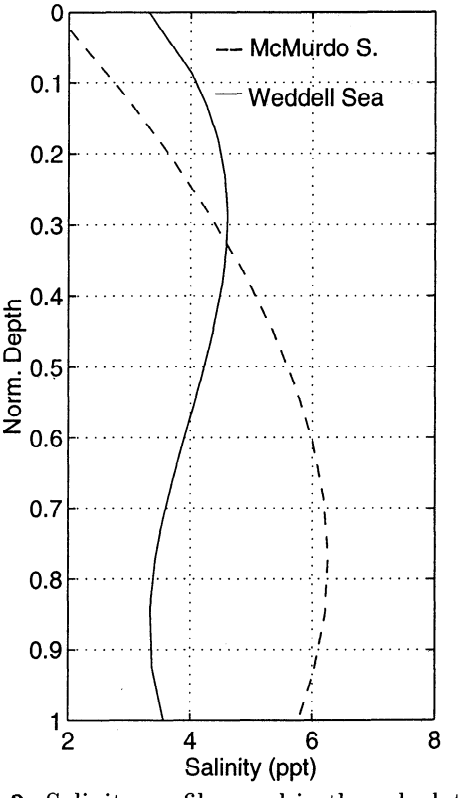

Figure 3. Salinity profiles used in the calculations for the Weddell Sea and for McMurdo Sound.

cussion of the influence of the sea ice temperature on the brine volume.

Divergence of irradiance. For different computer experiments, algae were considered to be homogeneously distributed within a single layer, positioned at the bottom (4, 10 or 20 cm thick) or near the top (20 cm thick) of the ice sheet (see Figures 6 and 13). In the interior of an algal layer the divergence of irradiance is given by

$$\frac{\partial F_i(z)}{\partial z} = -\int i(z_{\mathrm{alg}},\lambda)\,(K_{\lambda,\mathrm{ice}} + f\,K_{\lambda,\mathrm{alg}}) \times \exp[-(K_{\lambda,\mathrm{ice}} + K_{\lambda,\mathrm{alg}})\,(z - z_{\mathrm{alg}})]\,d\lambda \quad (17)$$

with $i(z_{\mathrm{alg}},\lambda)$ denoting the spectral irradiance entering into top of layer, $K_{\lambda,\mathrm{ice}}$ and $K_{\lambda,\mathrm{alg}}$ the extinction coefficients of sea ice and microalgae at wavelength λ, and z_{alg} the depth of the upper interface between pure sea ice and the algal layer. Energy transferred to photosynthesis is considered by the factor $f = 1 - \nu$, with ν being the photosynthetic efficiency. The photosynthetic efficiency is defined as the ratio of energy stored to energy absorbed. Since there are no field measurements from which ν could be directly determined, we estimate maximum and minimum values of ν utilizing the linear relationship between ν and the quantum yield ϕ [*Kirk*, 1983]

$$\nu = 1.97\,\phi \quad (18)$$

The quantum yield ϕ is defined as mole carbon accumulated per mole photons absorbed. When the theoretical maximum quantum yield $\phi_{\max} = 1/8$ is reached, $\nu_{\max}$ equals 0.25 [*Morel*, 1978]. Averaging measured maximum quantum yields (summarized by *SooHoo et al.* [1987]) results in a value of 1/13 for the quantum yield ϕ, corresponding to a photosynthetic efficiency $\nu = 0.15$. In other words, under most favorable conditions, 85% of the part of the energy that is absorbed by algal pigments is converted into heat, while 15% is stored as photochemical energy. On the other hand, only a fraction of the absorbed energy is transferred directly to photochemistry. First, absorption due to other particles like detritus may occur. Second, respiration of the algae was ignored, which in addition, releases a considerable fraction of the photochemical energy as heat. Therefore the maximum value for f is 1.0, indicating that the entire absorbed energy in the algal layer is converted to heat. In the model integrations, $f = 0.95$ was chosen, but to assess the effect of the storage of photosynthetic energy, calculations assuming $f = 0.85$ and $f = 1.0$ were included (see section 3.3). We neglected fluorescence in our estimation, because in living, photosynthesizing algal cells, only a very small proportion (~1%) of the absorbed light is lost by fluorescence [*Kirk*, 1983].

Ice-water interface. Once the temperature profile has been determined, the temperature gradient at the lower surface of the ice sheet $\partial T/\partial z|_{H+h_s}$ can be computed and bottom melting or accretion can be derived by an energy balance at the ice-water interface

$$\left.\frac{d(H+h_s)}{dt}\right|_{H+h_s} = \frac{1}{\rho L}\left(k\left.\frac{\partial T}{\partial z}\right|_{H+h_s} - F_w\right) \quad (19)$$

where F_w is the oceanic heat flux. F_w has been assumed to vary between 0 and 40 W m^{-2} in the Weddell Sea [*Eicken*, 1992].

In McMurdo Sound, platelet ice layers are often observed [e.g., *Dayton et al.*, 1969; *Grossi et al.*, 1987; *Jeffries et al.*, 1993]. Platelet ice layers commonly occur as aggregates of platy ice crystals up to 5 mm thick and 150 mm in diameter. They consist of about 20-50% ice and 50-80% seawater. The platelet layer (about 0.5 m thick) thermodynamically decouples the sea ice and the ocean [*Kipfstuhl*, 1991]. Since the water within the platelet layer is at the freezing point, a positive oceanic heat flux decreases the fraction of the ice in the platelet layer but does not directly affect the energy balance at the bottom of the ice, thus F_w is 0 in (19). Moreover, *Jeffries et al.* [1993] suggested a negative oceanic heat flux in McMurdo Sound through the flux of supercooled water from beneath the ice shelves associated with platelet ice formation, which explains why McMurdo Sound fast ice is thicker than Ross Sea pack ice (see also *Crocker and Wadhams* [1989]). For this reason and because the difference between model results for cases with or without an algal layer is not affected to a large degree by the oceanic heat flux, F_w was set to 0 in model simulations for McMurdo Sound. However, to assess the possible effect of a positive heat flux on model results, $F_w > 0$ was studied in section 3.3.

Equation (19) was used to calculate increased bottom melting rates as the absorption of light by algae and its conversion into heat increased the temperature gradient at the bottom of the ice sheet. The model was integrated on a CRAY computer using a forward explicit finite difference scheme. The grid spacing was 1 cm in the vertical coordinate, the time step was 36 s.

2.2. The Bio-optical Model

Incoming solar shortwave radiative fluxes are significantly reduced by absorption and scattering in the atmosphere and vary strongly with the time of day, season, and latitude. *Arrigo et al.* [1991] developed a bio-optical model which accounts for seasonal changes in the physical and biological processes influencing radiative transfer in sea ice. This model was modified, as described below, and coupled to the thermodynamic model of sea ice. The spectral range was extended from the visible (400 nm $< \lambda <$ 700 nm) to the near infrared ($\lambda <$ 4000 nm), to determine the total incoming shortwave flux. A parameterization of the effect of a cloud cover on the total irradiance was modified to take into account the effect of a cloud cover on spectral irradiance fluxes. A calculation of the divergence of irradiance (see (17)) in every layer of the model was included to permit the determination of additional heating of the ice, as light absorbed by microalgae is converted to heat.

Atmospheric irradiance model. Model simulations focus on the temporal development of the ice cover, including biophysical properties representative

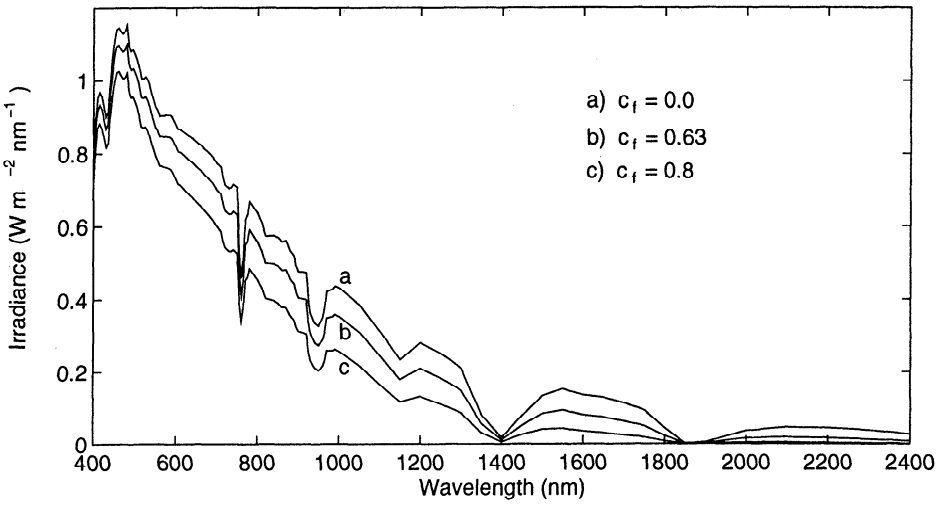

Figure 4. Incident irradiance on the sea ice surface for clear skies (cloud cover fraction $c_f = 0.0$). Incident irradiance for McMurdo Sound ($c_f = 0.63$) and for the Weddell Sea ($c_f = 0.8$) were determined by the parameterization (22); see text for details.

for McMurdo Sound and the Weddell Sea. Thus it was necessary to employ a time- and latitude-dependent atmospheric irradiance model, which permits the calculation of irradiance at the sea ice surface and within the sea ice for any given latitude, date of the year, and time (for results and discussion of the bio-optical model, see *Arrigo et al.* [1991] and section 3.1). In order to determine incident spectral fluxes during the model simulated season (about 5 months) as a function of the zenith angle, the spectral irradiance at the sea ice surface $F_R(\lambda)$ (Figure 4) is predicted by a simplified spectral atmospheric irradiance model [*Brine and Iqbal*, 1983].

Briefly summarized, the global spectral irradiance at the ice surface $F_R(\lambda)$ is given by the sum of a direct component and a diffusive component. The direct component is determined by calculating absorption and scattering of the extraterrestrial irradiance in the atmosphere due to processes like Rayleigh scattering, absorption by ozone, water vapor, mixed gases, and aerosols. Extraterrestrial irradiance was reported by *Thekaekara* [1973], and spectral absorption coefficients were taken from *Leckner* [1978]. The calculation of the diffusive component includes ground reflection, aerosol scattering, and Rayleigh forward scattering (for details, see *Brine and Iqbal* [1983]). The employed atmospheric irradiance model by Brine and Iqbal simplifies processes of radiation transfer in the atmosphere. Nevertheless, the model sufficiently describes the incident irradiance at the sea ice surface (see section 3.1).

The direct and the diffusive component of irradiance are functions of the cosine of the zenith angle θ, which is calculated from the standard geometric formula [e.g., *Kirk*, 1983]

$$\cos\theta = \sin\varphi \sin\delta - \cos\varphi \cos\delta \cos\tau \qquad (20)$$

where φ, δ, and τ are latitude, declination, and hour angle, respectively. The hour angle τ equals $2\pi \times$ time of day $\times (24 \times 3600)^{-1}$, and the latitude is 77°50'S for McMurdo Sound and 63°21'S for the northwestern Weddell Sea, respectively. The declination δ was determined from formulas given by *Spencer* [1971].

Cloud cover. Cloud cover reduces the total irradiance and affects the spectral distribution of the incident irradiance at the sea ice surface [*Grenfell and Perovich*, 1984]. The empirical parameterization by *Parkinson and Washington* [1979] is commonly used to describe the influence of the cloud cover fraction c_f on the total incoming shortwave radiation F_R

$$F_R = F_{R0}(1 - 0.6\, c_f{}^3), \qquad (21)$$

where F_{R0} is the global shortwave radiation under cloudless skies. The parameterization for the total irradiance (21) was modified to account for the effect of a cloud cover on spectral irradiance, because a spectral decomposition of incoming shortwave radiation is included in this model.

The spectral irradiance at the sea ice surface is decreasing rapidly at longer wavelengths (>1000 nm), when a cloud cover is present. Since a function of the form $\exp(-\lambda^2)$ decreases rapidly at longer wavelengths, the spectral irradiance for clear skies at wavelength λ was multiplied by $\exp[-A(c_f)\,\lambda^2]$, with $A(c_f)$ being a cloud factor determined by (22). This consideration yielded better agreement with measured spectra (compare Figure 4 and *Grenfell and Perovich* [1984, Figure 8]) than that obtained by the reduction of the incident irradiance by a constant factor (independent of the wavelength). Furthermore, we ascertained that this parameterization is consistent with (21), since the cloud factor $A(c_f)$ was numerically determined from

$$F_R = F_{R0}(1 - 0.6\, c_f{}^3) = \int F_R(\lambda) \exp[-A(c_f)\,\lambda^2]\, d\lambda \qquad (22)$$

where $F_R(\lambda)$ is the spectral irradiance at the sea ice surface for clear skies (determined using the bio-optical model). Thus the parameterization (22) does not

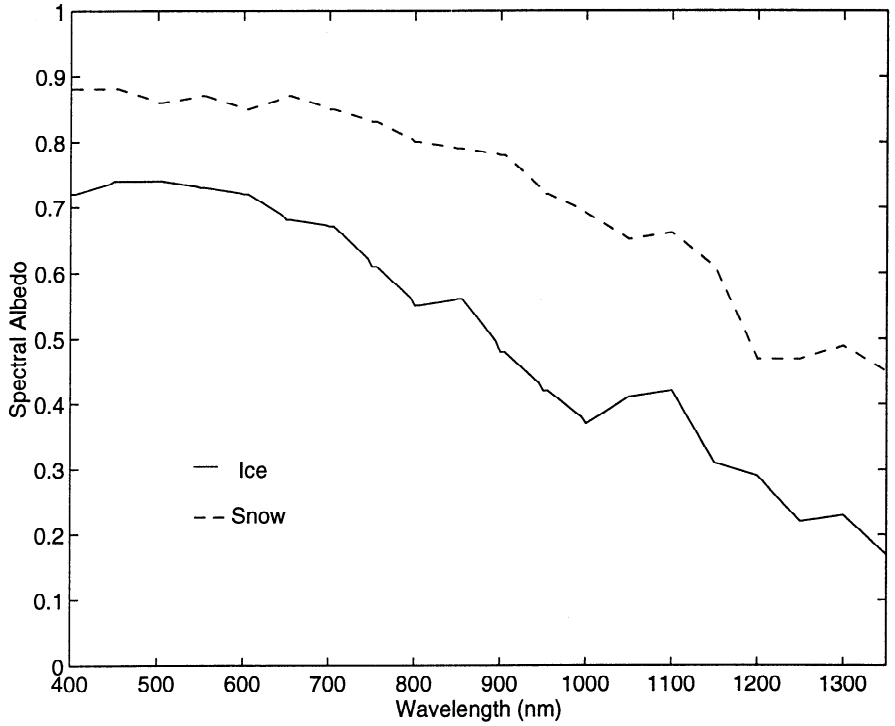

Figure 5. Spectral albedos for ice and snow in the spectral range from 400 to 1350 nm [*Schlosser*, 1988].

merely include the reduction of the total irradiance by a cloud cover, according to (21), but also takes the enhanced influence of clouds on the spectral irradiance for higher wavelengths into account. For the simulations in the Weddell Sea and the corresponding cloud cover fraction $c_f = 0.8$, $A(c_f)$ was determined to be 5.24×10^{-7}, while $A(c_f)$ was 2.02×10^{-7} for $c_f = 0.63$ in McMurdo Sound.

Albedo and attenuation. Values for the spectral albedo α_λ are based on measurements by *Schlosser* [1988] in the spectral range from 400 to 1350 nm (Figure 5). A parameterization for α_λ was taken from *Ebert and Curry* [1993] in the spectral range from 1350 to 4000 nm (Table 2). The attenuation of spectral irradiance by snow, sea ice, and microalgae is described by Beer's law

$$i(z, \lambda) = i(z_0, \lambda)\, e^{-K_\lambda z} \tag{23}$$

with spectral irradiance $i(z, \lambda)$ at depth z and wavelength λ; z_0 is the depth of the upper boundary of the snow, sea ice, or algal layer (see Figure 13); and K_λ is the extinction coefficient of the corresponding medium.

Table 2. Spectral Albedos in the Near Infrared

Surface Type	Band 1, 1350-2380 nm	Band 2, 2380-4000 nm
Snow		
Direct	$0.384\text{-}0.222\mu$	$0.053\text{-}0.047\mu$
Diffuse	0.25	0.025
Sea ice	0.055	0.036

Values are taken from *Ebert and Curry* [1993]. Here $\mu = \cos(\theta)$ is the cosine of the zenith angle.

Extinction coefficients for ice and snow have been taken from *Grenfell and Maykut* [1977]. Because backscattering by algal particles has been ignored, the spectral extinction coefficient due to particles can be approximated by [*Arrigo et al.*, 1991]

$$K_{\lambda,\mathrm{alg}} = \frac{C_{m^3}\, a^*_\lambda}{\bar{\mu}}, \tag{24}$$

with chlorophyll a concentration C_{m^3} (mg chl a m^{-3}) and a^*_λ the chl a specific absorption coefficient [m^2 (mg chl a)$^{-1}$]; $\bar{\mu} = 0.656$ is the mean cosine of the angular distribution of irradiance [*Grenfell*, 1983]. The chl a specific absorption coefficient a^*_λ (Figure 6d) was determined by in situ measurements [*Perovich et al.*, 1993]. Differences appear when in situ values of a^*_λ are compared to in vivo values, presumably because the geometric distribution of algae in the ice column is not preserved in meltwater suspensions or because dissolved organics are excluded in in vivo measurements [*Perovich et al.*, 1993]. Furthermore, differences for a^*_λ are apparent for a variety of sea ice microalgal species [*Arrigo et al.*, 1991]. However, the direct absorption spectra (Figure 6d) are comparable to the inferred values reported by *Maykut and Grenfell* [1975] and to the laboratory measurements of *SooHoo et al.* [1987] and *Arrigo et al.* [1991].

3. Model Results

3.1. Test of the Bio-optical Model

Because a validation of the bio-optical model is a prerequisite for a convincing discussion of different integrations of the coupled model, a test of the bio-optical

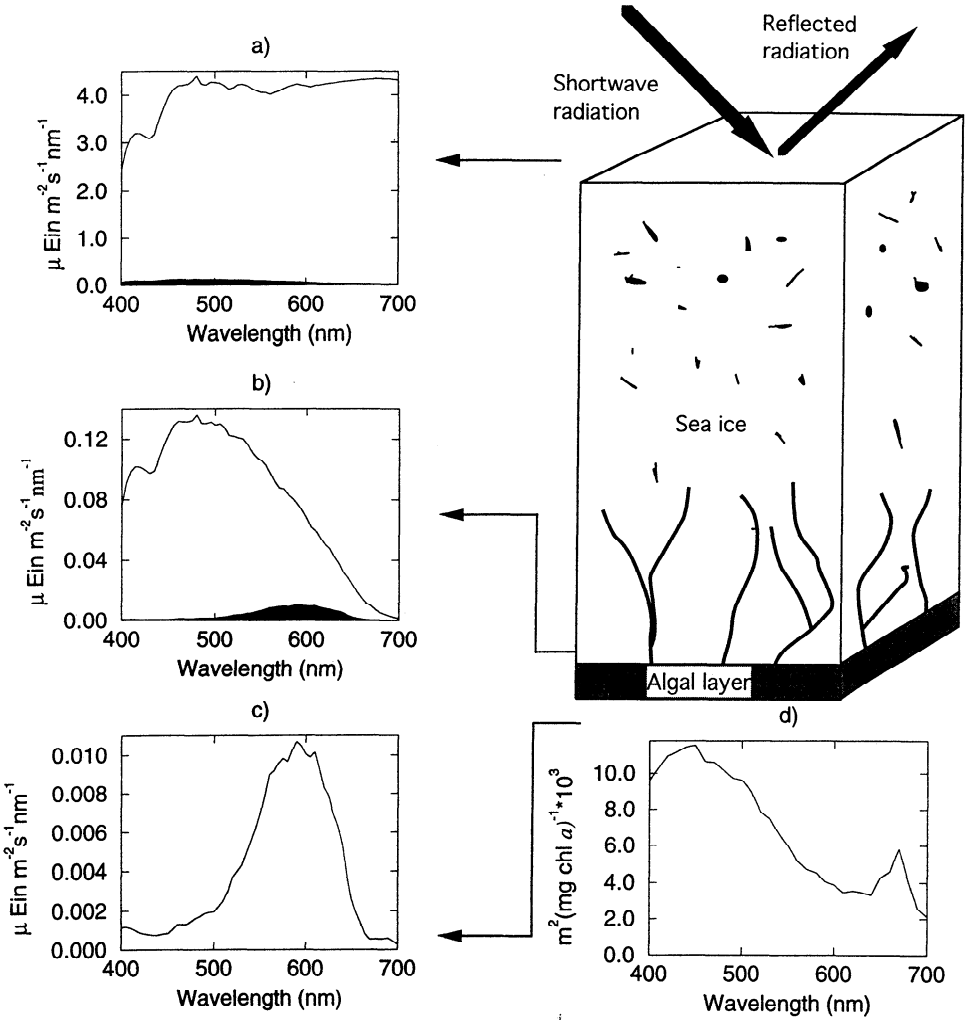

Figure 6. Model results for the light attenuation by sea ice and microalgae in McMurdo Sound on December 12. Spectral incident irradiance (a) on the surface, (b) above the algal layer after passing through 1.8 m of sea ice, and (c) just below the algal layer (note the change in the scale of the vertical axes). Total irradiance in the visible range (400-700 nm) is 1216 μ E m^{-2} s^{-1} in Figure 6a, 25 μ E m^{-2} s^{-1} in Figure 6b and 1.2 μ E m^{-2} s^{-1} in Figure 6c. Shaded areas in Figures 6a and 6b are expanded in Figures 6b and 6c, respectively. (d) In situ absorption spectrum of microalgae [*Perovich et al.*, 1993].

model is presented first. Figure 6 shows model results for the attenuation of light in the visible range from 400 to 700 nm by the ice and by microalgae for a simulation of the conditions in McMurdo Sound on December 12 at 1351 LT. The snow depth was 0 cm; algal standing stock at the bottom of the congelation ice was 300 mg chl a m^{-2}. Incident irradiance on the ice surface (Figure 6a) is 1216 μ einsteins (E) m^{-2} s^{-1} (270 W m^{-2}). Since model results are compared to measured values reported in units of einsteins by *SooHoo et al.* [1987], irradiance values in watts had to be expressed in units of einsteins in this case. The conversion from μ E m^{-2} s^{-1} into W m^{-2} is

$$i^W(\lambda) = i^\mu(\lambda) \times 10^{-6} \times \frac{N_A\, h\, c}{\lambda} \qquad (25)$$

with $i^W(\lambda)$ and $i^\mu(\lambda)$ the spectral irradiance in W m^{-2} nm^{-1} and μ E m^{-2} s^{-1} nm^{-1}, respectively. N_A = 6.022×10^{23} mol^{-1} is Avogadros constant, $h = 6.626 \times 10^{-34}$ J s is Planck's constant, and $c = 2.998 \times 10^8$ m s^{-1} is the speed of light. The total irradiance is calculated by integrating (25) over all wavelengths.

After passing through 1.8 m of sea ice (Figure 6b), total irradiance is reduced to about 25 μ E m^{-2} s^{-1} (7 W m^{-2}). Furthermore, the high attenuation by sea ice at longer wavelengths shifts the maximum of the spectrum to 500 nm. Beneath the algal layer (Figure 6c), quanta are concentrated between 580 and 620 nm. Total irradiance has decreased to 1.2 μ E m^{-2} s^{-1} (0.3 W m^{-2}). The maximum at 600 nm corresponds to a minimum in the absorption spectrum of the ice algae (Figure 6d). Absorption centered at 440 and 670 nm is due to chl a, while the attenuation between 450 and 550 nm is due to chl c and carotenoid accessory pigments, particularly fucoxanthin [*Perovich et al.*, 1993].

Figure 7 shows comparable results from measure-

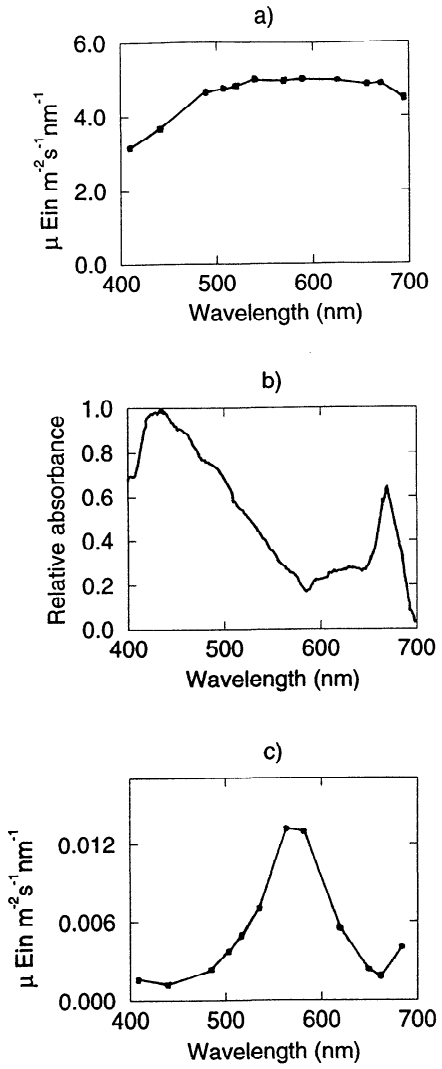

Figure 7. Spectral irradiance measured by *SooHoo et al.* [1987] in McMurdo Sound on December 12. (a) Incident irradiance on the surface of ice, with total irradiance of 1364 μ E m^{-2} s^{-1}. (b) In vivo absorption spectrum of microalgae from bottom 20 cm of fast sea ice. (c) Spectral irradiance measured just under the algal layer, with total irradiance having decreased to 1.379 μ E m^{-2} s^{-1}.

ments carried out in McMurdo Sound on December 12 at 1351 LT [*SooHoo et al.*, 1987]. Incident irradiance on the sea ice surface is 1364 μ E m^{-2} s^{-1}. The model predicts about 90% of this value (1216 μ E m^{-2} s^{-1}). The difference between model results and observational data may be explained by the model's use of a comparatively simple spectral atmospheric irradiance calculation. Air mass, which is only computed as a function of zenith angle, significantly affects the total irradiance at the sea ice surface and cannot be reproduced exactly by the model for particular atmospheric conditions at a given time of day.

Beneath the algal layer, total irradiance is 1.4 μ E m^{-2} s^{-1} (Figure 7c), while it is 1.2 μ E m^{-2} s^{-1} in the model (Figure 6c). However, if the total irradiance at the surface is set to 100% in the model and in measurements, the fraction of incident irradiance that penetrates the algal layer is 0.099% in the model results and 0.10% in the field observations. The maximum of transmitted radiation predicted by the model is shifted toward longer wavelengths (Figure 6c) when compared with the data of *SooHoo et al.* [1987] (Figure 7c). This shift is due to the absorption spectrum of microalgae used in the model (Figure 6d) [*Perovich et al.*, 1993], which is also displaced to the longer wavelengths when compared with the absorption spectrum measured by *SooHoo et al.* [1987] (Figure 7b). Despite slight differences between model results and field measurements, the model adequately reproduces total irradiance and the spectral distribution of light at the ice surface, in the interior of the ice, and beneath the algal layer. As can be seen from Figures 6b and 6c, about 24 μ E m^{-2} s^{-1} (7 W m^{-2}) are absorbed by the algal layer (note that this value varies with chl *a* concentration and incident irradiance). This absorbed energy, which would otherwise penetrate the whole ice sheet and enter the water column, must be considered as a contribution to the heat budget of sea ice that affects the melt rate at the bottom of the ice sheet.

3.2. Modeling the Ice Thickness Evolution

A particular goal of this work is to clarify the influence of high algal biomass concentrations restricted to the lower portion of sea ice on bottom melting. In order to address this question, we present model results of the coupled model using input parameters reported by *SooHoo et al.* [1987], which had been employed to test the bio-optical model (see section 3.1), including high algal biomass of 300 mg chl *a* m^{-2}. Since the accumulation and the distribution of algal biomass exhibit high temporal and spatial variability, we will discuss the effect of this parameter (and others) in a later section. Development of sea ice thickness in McMurdo Sound for algal free ice and for ice with an algal standing stock of 300 mg chl *a* m^{-2} is shown in Figure 8. Ice thickness increases until the beginning of December (day 340, thickness about 200 cm), when bottom melting starts. Bottom melting results in a successive release of algal biomass into the water column and, consequently, in a decrease of the algal standing stock, which was accounted for in the model. The final ice thickness on February 4 was 198 cm for the algal free ice and 194 cm for the ice containing algae. The physical reason for the enhanced melting rate is an increase of the temperature gradient in the lower layers of the ice brought on by the additional absorption of light and its conversion into heat by the algae.

Irradiance and temperature profiles. On December 17, total irradiance at the depth of the ice-algal layer interface (Figure 9a) was about 4.5 W m^{-2} in both algal free ice and ice containing algae. At the ice-water interface, total irradiance has decreased to less than 1 W m^{-2} for the ice containing algae (Figure 9a, solid line), whereas total irradiance was about 3.5 W m^{-2} for the algal free congelation ice (Figure 9a, dashed line).

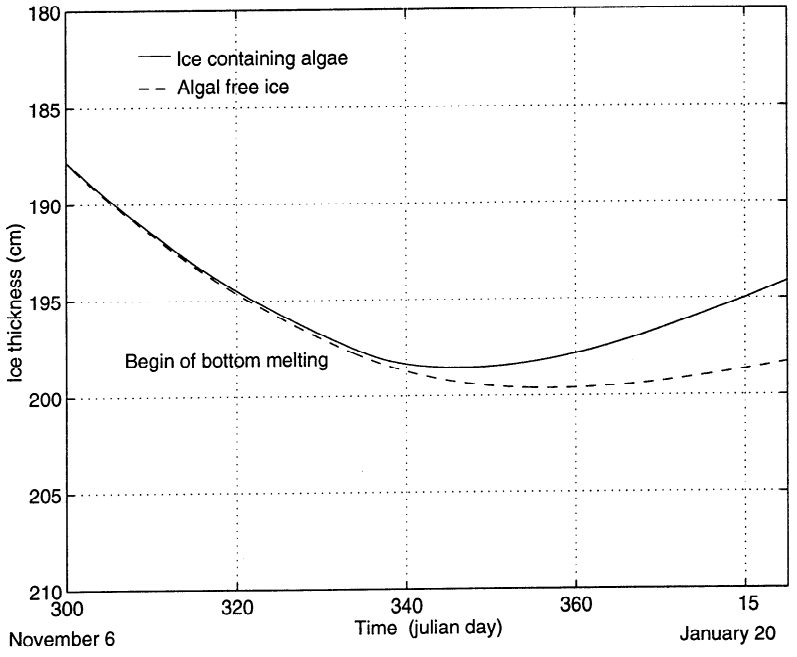

Figure 8. Model results for the development of sea ice thickness in McMurdo Sound. Ice thickness increases until the beginning of December (day 340), when bottom melting starts. In comparison to the model run with algal free ice (final thickness 198 cm), an increase in the melt rate at the bottom of the ice was calculated in a model run with an algal standing stock of 300 mg chl a m^{-2} (final thickness 194 cm).

The key variable that provides the link between light absorption by microalgae and sea ice temperature is the divergence of irradiance $\partial F_i(z)/\partial z$ (see (9)). Since the problem is one-dimensional, the divergence of irradiance is the derivative of the irradiance with respect to z (neglecting the storage of photosynthetic energy). For algal free ice, $\partial F_i(z)/\partial z$ is nearly constant (Figure 9b, dashed line), corresponding to the linear decrease of the total irradiance (Figure 9a, dashed line). In contrast, for the ice containing algae a pronounced maximum in $\partial F_i(z)/\partial z$ occurred at the top of the algal layer (Figure 9b, solid line), where total irradiance exhibited the greatest change (Figure 9a, solid line).

Consequently, the temperature profile for the algal free ice increased almost linear with depth (Figure 10a, dashed line). In contrast, a maximum in the temperature profile for ice containing algae occurred approximately 2 cm beneath the ice-algal layer interface (Figure 10a, solid line) due to the peak in the divergence of irradiance at the top of the algal layer (Figure 9b, solid line). Since heat is transported away through heat conduction by diffusion, the maximum in the temperature is less pronounced than the maximum in the divergence of irradiance.

It follows from the positive temperature gradient at the bottom of algal free ice that the ice sheet was growing in thickness on December 17 (see (19)). On the other hand, the temperature gradient at the bottom of algae-containing ice was negative, indicating that bottom melting had already started. In summary, the en-

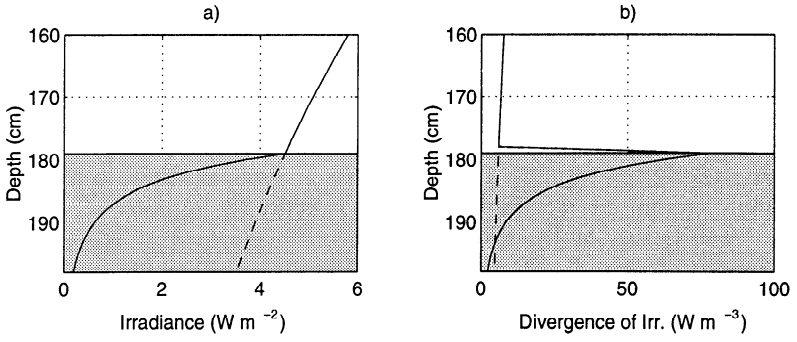

Figure 9. Model results for the (a) total irradiance and (b) divergence of irradiance in the lower portion of sea ice for algal free ice (dashed line) and ice containing algae (solid line) for a simulation in McMurdo Sound on December 17. The algal layer is represented by the shaded area.

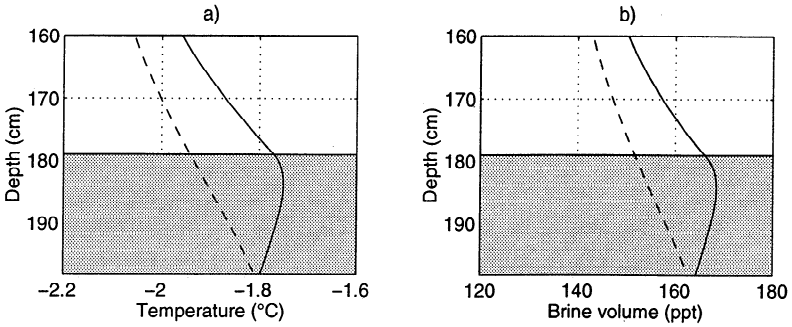

Figure 10. Model results for the (a) sea ice temperature and (b) brine volume, corresponding to Figure 9. Sea ice salinity is about 6 ppt and is nearly constant in the lower part of the ice for model simulations in McMurdo Sound.

hanced light absorption in the algal layer was responsible for the peak in the divergence of irradiance at the interface between pure ice and the algal layer. The heat released at this point produced the maximum in the temperature profile and enhanced the melt rate via the temperature gradient at the bottom of the ice sheet.

Brine volume and bottom melting. Since the sea ice salinity is nearly constant in the lower portion of the ice (~6 ppt in model calculations for McMurdo Sound), the brine volume (Figure 10b) closely follows the temperature profile (Figure 10a). The brine volume for ice containing algae is generally higher (168 ppt at $z = 182$ cm) in comparison to algal free ice (152 ppt at $z = 182$ cm). The increased brine volume may weaken the ice and enhance brine and nutrient fluxes in the lower portion of the ice.

The calculated temperature and brine volume maximum at the top of the algal layer suggests intensified internal melting at this site and may promote an episodic loss of the entire 20-cm-thick algal layer into the water column. However, this scenario appears to be unlikely. The sea ice temperature of about −1.7°C is far below the melting point of about −0.3°C and −0.5°C at a salinity of 6 and 10 ppt, respectively. Furthermore, the brine volume increases almost linearly from 164 ppt at the bottom to 168 ppt at the top of the algal layer, indicating that increased brine volume occurs within the entire algal layer and is not restricted to the top.

Internal temperature and brine volume maxima at the top of the algal layer are rather likely to increase bottom melting. The temperature at the bottom of the ice is fixed at −1.8°C, and the increased sea ice temperature at the ice-algal layer interface results in a steep temperature gradient at the bottom, which in turn enhances the bottom melt rate. To estimate the effect of a rise in temperature at the top of the algal layer on bottom melting, the bottom melt rate $\partial H/\partial t$ can be calculated according to (19). Let us suppose that the thickness of the algal layer equals 4 cm, because a thin algal layer (high algal concentration) is needed to produce a strong temperature maximum. If $T(z) = -0.8$°C at the top of the layer and $T(z) = -1.8$°C at the bottom, $\partial T(z)/\partial z$ is approximately 25 K m^{-1}, and the predicted bottom melt rate would be as follows:

$$\frac{\partial H}{\partial t} = \frac{k}{L\rho}\frac{\partial T(z)}{\partial z} = 1.58\,\text{cm d}^{-1},$$

assuming the latent heat of melting $L = 283 \times 10^3$ J kg^{-1}, the sea ice density $\rho = 917$ kg m^{-3} and the thermal conductivity $k = 1.9$ W m^{-1} K^{-1}. The selected values for L, ρ, and k are representative for a sea ice temperature at the ice-water interface of −1.8°C and a sea ice salinity of 6 ppt (the salinity at the bottom of the ice sheet in model calculations for McMurdo Sound was about 6 ppt; see Figure 3). Thus the entire algal layer is melted off from the bottom up after only 2.5 days. This example demonstrates that an internal temperature and brine volume maximum at the top of the algal layer is accompanied by massive bottom melting and a successive release of the entire algal biomass from the bottom of the ice before the increased brine volume results in a sufficient decrease of mechanical strength at the ice-algal layer interface to cause a loss of the algal layer as a whole.

Analytical calculation of Δz. The difference in ice thickness (Figure 8) brought about through light absorption by microalgae was about 4 cm based on solving the heat conduction equation. A simple calculation of the entire ice volume that can be melted by the algae yields nearly the same result. The mean total irradiance above the algal layer is about 4 W m^{-2} during the time of melting from mid-December to mid-January (determined using the bio-optical model). If this energy is completely converted into latent heat to melt the ice, the thickness Δz of the melted ice layer is given by

$$\Delta z = \frac{I(z_{\text{alg}})t}{L\rho} \tag{26}$$

with total irradiance $I(z_{\text{alg}}) = 4$ W m^{-2}, the depth of the ice-algal layer interface $z_{\text{alg}} \approx 1.8$ m, time $t = 40$ days, density $\rho = 917$ kg m^{-3}, and latent heat of melting $L = 283 \times 10^3$ J kg^{-1}. The value of L corresponds to the latent heat of melting required for the complete melting of sea ice, starting at a temperature of −2°C and a salinity of 6 ppt. Thus Δz is 5.3 cm. This value is slightly higher than the value of 4 cm predicted by the thermodynamic model, because we assumed in the sim-

ple calculation that the entire absorbed energy is used to melt the ice, not taking the heat conduction and the storage of photosynthetic energy into account.

3.3. The Response to Variations in Model Parameters

Input parameters of the model such as the sea ice thickness, the algal standing stock, and the thickness of the algal layer are quantities which are likely to affect the bottom melt rate. In the model integration, corresponding to measurements of *SooHoo et al.* [1987], the mean ice thickness was 195 cm, algal standing stock was 300 mg chl *a* m^{-2}, and the thickness of the algal layer was 20 cm. Nevertheless, a variety of values for these parameters have been reported. From 1980 to 1989 the observed sea ice thickness in McMurdo Sound ranged from 150 to 270 cm [*Arrigo et al.*, 1993] and the reported algal standing stocks in the bottom ice habitat varied between 5 and 600 mg chl *a* m^{-2} [*SooHoo et al.*; 1987; *Palmisano et al.*, 1988; *Dieckmann et al.*, 1992]; *Palmisano and Sullivan* [1983] reported a mean value of 131 mg chl *a* m^{-2} (656 mg m^{-3}) in the bottom 20-cm ice section of congelation ice. Differences in the thickness of the bottom ice habitat also have been reported. Whereas *SooHoo et al.* [1987] observed a 20-cm-thick congelation ice algal layer in McMurdo Sound, other authors reported high algae concentrations restricted to the bottom 1- to 5-cm portion of sea ice [*Palmisano et al.*, 1985; *Arrigo et al.*, 1993]. To estimate the effect of sea ice thickness H, algal standing stock, and thickness of the algal layer h_a on bottom melting, additionally melted ice Δz was calculated for environmentally relevant values of these parameters.

The influence of the thickness of the algal layer. The influence of the thickness of the bottom ice habitat h_a on Δz was studied separately by diminishing the vertical dimension of the algal layer, while keeping the algal standing stock and the sea ice thickness constant, corresponding to the values reported by *SooHoo et al.* [1987]. To avoid numerical problems, a minimum h_a of 4 cm was chosen (grid spacing 1 cm). A reduction of h_a from 20 to 10 cm and from 20 to 4 cm results in an increase in Δz from 4.1 to 5.5 cm and from 4.1 to 5.4 cm, respectively. Since algal concentration increases with a decrease in h_a (note that the algal standing stock is constant) and the internal temperature maximum at the ice-algal layer interface is shifted toward the ice bottom (see Figure 10a), the temperature gradient in the lower layers of the ice shows a strong increase, resulting in more rapid melting. The result that a thinner algal layer (4 cm) leads to less melted ice at the end of the integration on January 20 than the thicker algal layer (10 cm) is easily understood by following the time series of melting (Figure 11). When h_a is 4 cm, melting occurs rapidly and the entire algal layer is melted off after only 35 days; subsequently, the melting rate slows down (day 10, thickness 194 cm).

The influence of H, h_a, and the algal standing stock. The normalized difference in the sea ice

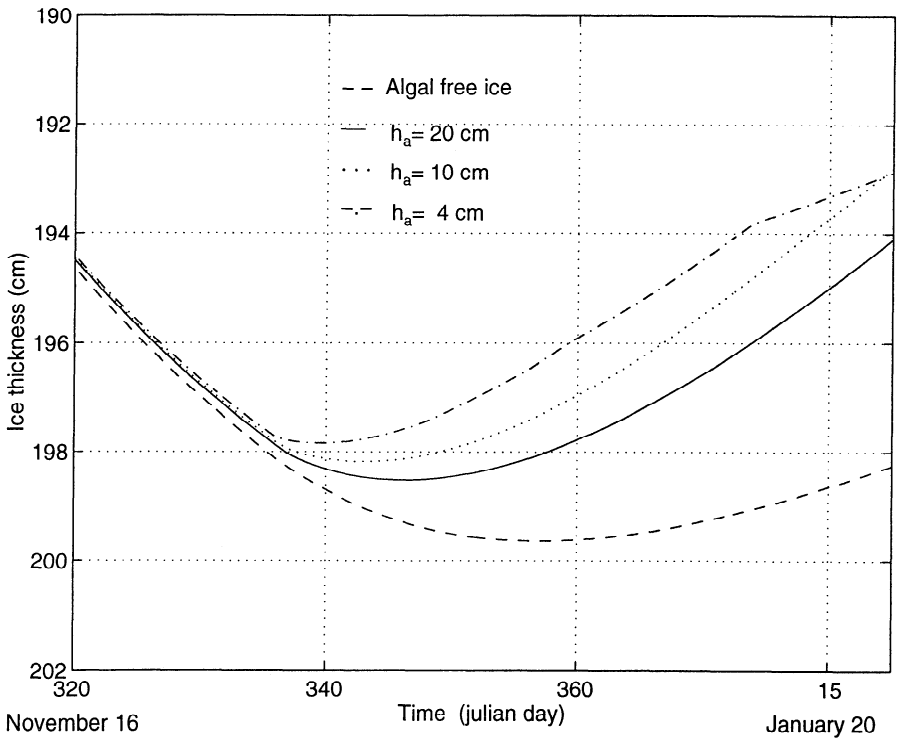

Figure 11. Development of sea ice thickness for a variation of the thickness of the algal layer h_a. The melt rate increases with decreasing h_a. When $h_a = 4$ cm, the entire algal biomass is released into the water column after only 35 days. Subsequently, the melt rate slows down (day 10, sea ice thickness 194 cm).

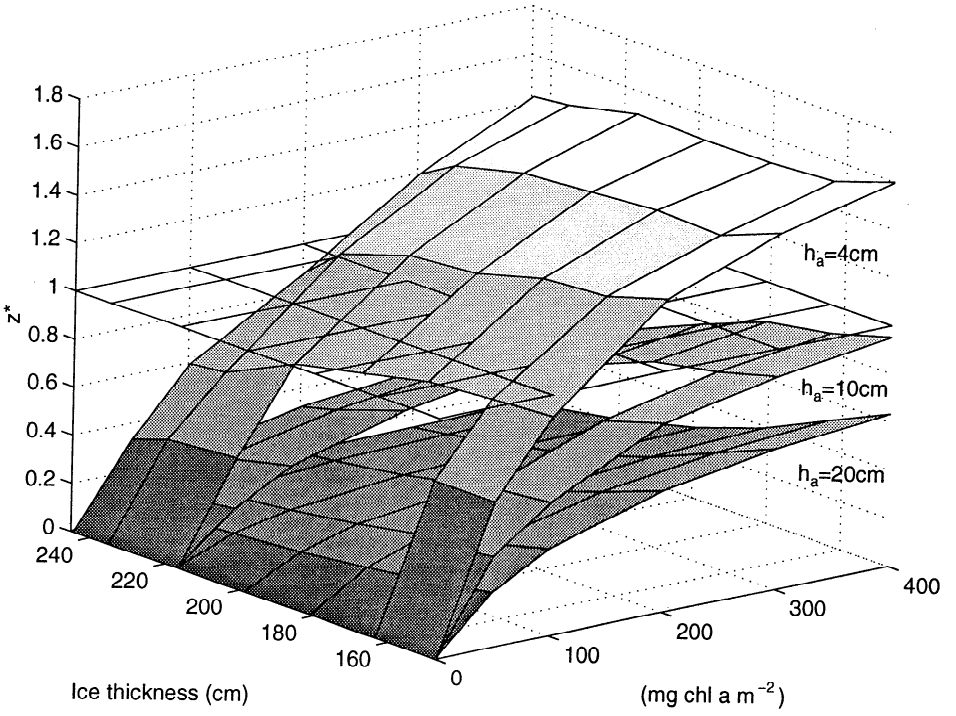

Figure 12. Model results for the normalized difference in the sea ice thickness ($z^* = \Delta z/h_a$) as a function of the algal standing stock, the sea ice thickness H, and the thickness of the algal layer h_a. The ability of the algae to hasten bottom melting and thus to increase z^* may solely occur for high algal standing stocks and small sea ice thicknesses, when the algal layer is thick (h_a = 20 cm). On the other hand, a significant increase in z^* may also occur for small algal standing stocks, when the algal layer is thin (h_a = 4 cm).

thickness ($z^* = \Delta z/h_a$) as a function of all three essential parameters (H, h_a, and the algal standing stock) at the end of the model integration on January 20 is summarized in Figure 12. The quantity z^* represents a key variable. If z^* exceeds the value 1.0 (marked by the grid in Figure 12), then the additional ice melted through light absorption by microalgae exceeds the thickness of the algal layer. Thus Figure 12 provides a tool to determine under which conditions of H, h_a, and the algal standing stock, ice melting may result in complete destruction of the microalgal habitat.

For h_a = 20 cm, z^* is always below 1.0, indicating that the entire algal layer cannot be melted off within the selected ranges of H and the algal standing stock. Nevertheless, a considerable amount of ice may be melted off as a result of light absorption by microalgae, up to a maximum of 60% (12 cm) of the microalgal habitat, when H = 140 cm and the algal standing stock is 400 mg chl a m^{-2}. The surface illustrating z^* for h_a = 20 cm approached a saturation value of about 0.6 as algal standing stock approached 400 mg chl a m^{-2}. This stems from the fact that the maximal heat release through light absorption by microalgae (for a given sea ice thickness) is limited by the light energy available at the depth of the algal layer (see (26)). As algal standing stock increases at any given H, a point is reached above which all of the available light energy is absorbed by microalgae and the maximum bottom melt rate is achieved.

Algal standing stock and concentration. For a thickness of the algal layer of 10 cm, z^* approaches the value 1.0, only for high algal standing stocks and small sea ice thicknesses (Figure 12). On the other hand, z^* exceeds 1.0 also for an algal standing stock of 100 mg chl a m^{-2} (H = 140 cm) and 200 mg chl a m^{-2} (H = 240 cm), respectively, if the algal layer is thin (h_a = 4 cm). What these results demonstrate is that H determines the percentage of surface light reaching the algal layer, whereas the algal standing stock determines the overall absorption of available light within the algal layer. The vertical dimension h_a over which energy is released as heat determines the distance of the heat source from the ice-water interface and the intensity of light attenuation within the algal layer at depth z, thereby regulating the effectiveness of released heat on bottom melting.

For H = 240 cm there is no significant increase in z^* for the thick algal layer (20 cm), while z^* increases dramatically for the thin algal layer (4 cm). Even though the algal standing stock ranges from 0 to 400 mg chl a m^{-2} in both cases, the concentration of algae dominates the effect on bottom melting for thick ice and must be distinguished from the algal standing stock. Both values are connected by the distribution of algal biomass within the ice, which in the case of a homogeneous distribution within an algal layer of a certain thickness h_a is given by

$$C_{m^3}(z) = \frac{C_{m^2}}{h_a} \tag{27}$$

where $C_{m^3}(z)$ is the algae concentration at depth z and C_{m^2} is the algal standing stock.

Unfortunately, most authors report algae concentrations in depth intervals of approximately 20 cm, implying that h_a is about 20 cm, thereby masking the existence of extreme concentrations within the bottom few centimeters of congelation ice. In contrast, *Smith et al.* [1990] determined the fine structure of the bottom ice habitat with a vertical resolution of about 2 mm at a site in the Canadian high Arctic. The layer of high chl *a* concentration was restricted to the bottom 1 cm of the ice, reaching values of 3000-60,000 μg L^{-1} at the ice-water interface, while the algal standing stock ranged from less than 5 to about 200 mg chl *a* m^{-2} during the time of observation.

Even though these data have been collected in the Arctic, they demonstrate that algal concentrations and thus the extinction coefficient of the algal layer can drastically be increased for thin algal layers (note the inverse relationship between $C_{m^3}(z)$ and h_a in (27)). Such an effect can only be observed, however, if the fine structure of the bottom ice habitat is investigated.

Sensitivity to other input parameters. In this section we investigate the extent to which the oceanic heat flux F_w, the relative humidity f_h, and the heat conversion factor of the algae f affect the outcome of the model integrations. We focus on these parameters because they are not well known or likely to affect the difference between model runs including and excluding microalgae in the numerical scheme. Furthermore, we focus on the response of the additionally melted ice Δz to changes in parameters for the model run corresponding to conditions in McMurdo Sound reported by *SooHoo et al.* [1987] (see section 3.2). The results obtained from different model runs, varying one parameter at a time within a plausible range, are listed in Table 3.

Because a positive heat flux causes higher bottom melt rates in model runs for algal free ice as well as for ice containing algae, the response of Δz to changes in the oceanic heat flux is small. The ice thickness of about 170-200 cm typically observed in the late spring in McMurdo Sound was not achieved in model runs assuming $F_w > 10$ W m^{-2} [cf. *Crocker and Wadhams*, 1989]. Therefore a maximum oceanic heat flux of 10 W m^{-2} was chosen. Varying F_w from 0 to 10 W m^{-2} caused 10% variations in Δz. An oceanic heat flux of $F_w = 10$ W m^{-2} resulted in a smaller Δz (4.2 cm) than $F_w = 5$ W m^{-2} ($\Delta z = 4.5$ cm), demonstrating that the algal layer was melted off more rapidly through the higher oceanic heat flux. Subsequently, the melting rate slowed down, similar to the effect of a higher bottom melt rate, caused by a smaller algal layer (see Figure 11). The influence of the relative humidity f_h is negligible. The latent heat flux is a function of the relative humidity (see (7)) and influences the surface temperature via the surface energy balance. The calculated Δz indicate that the bottom melt rate is not affected to a large degree by small variations in the surface temperature. The additionally melted ice Δz is 4.1 and 4.2 cm, assuming $f_h = 0.7$ and $f_h = 0.9$, respectively.

The sensitivity of Δz due to changes in the factor f, describing the heat conversion through light absorption by microalgae, exhibits an almost linear trend. A 5% and 15% reduction of f results in a 7% and 18% decrease in Δz ($f = 1.0$ indicates that 100% of the absorbed energy is converted to heat). This near-linear relationship between Δz and f provides an estimation for the influence of f on bottom melting and indicates that the model's outcome is not extremely sensitive to this parameter within the range of the theoretical minimum value (0.85) and the maximum value (1.0) of f.

Table 3. The Influence of Different Parameters on Additionally Melted Ice Δz

Value	Δz, cm
F_w	
0 W m^{-2}	4.1*
5 W m^{-2}	4.5
10 W m^{-2}	4.2
f_h	
70%	4.1
80%	4.1*
90%	4.2
f	
0.85	3.6
0.95	4.1*
1.0	4.4

F_w is oceanic heat flux, f_h is relative humidity, and f is the heat conversion factor of the algae.

* These values were used for the reference run.

3.4. Effects on Sea-Ice Porosity

In the Antarctic, high concentrations of algal biomass at or near the surface of sea ice are often observed, mostly due to processes associated with the flooding of the ice cover. Simulations were carried out to investigate the effect of such surface communities on the thermal regime of sea ice (Figure 13a). A 20-cm-thick algal layer was included in the numerical scheme. The layer was positioned at the top of the ice sheet, below the snow cover. The model was integrated from the end of the winter to the beginning of the summer, simulating light conditions for 63°S and forced by air temperature data for the Weddell Sea [*Kottmeier and Hartig*, 1990]. Model results for sea ice temperature and brine volume on December 23 are plotted in Figures 13b and 13c, respectively. The snow depth was 5 cm, and the algal standing stock was 250 mg chl *a* m^{-2}. The temperature profile for the algal free ice is almost linear, while an internal temperature maximum was calculated for the ice containing algae. The difference in sea ice temperature at a depth of 12 cm was 0.33 K.

However, such comparatively small changes in sea ice temperature correspond to more dramatic changes in brine volume. The specific heat of sea ice increases sharply, when T approaches 0°C, because absorbed energy is expended by internal melting. As brine volume

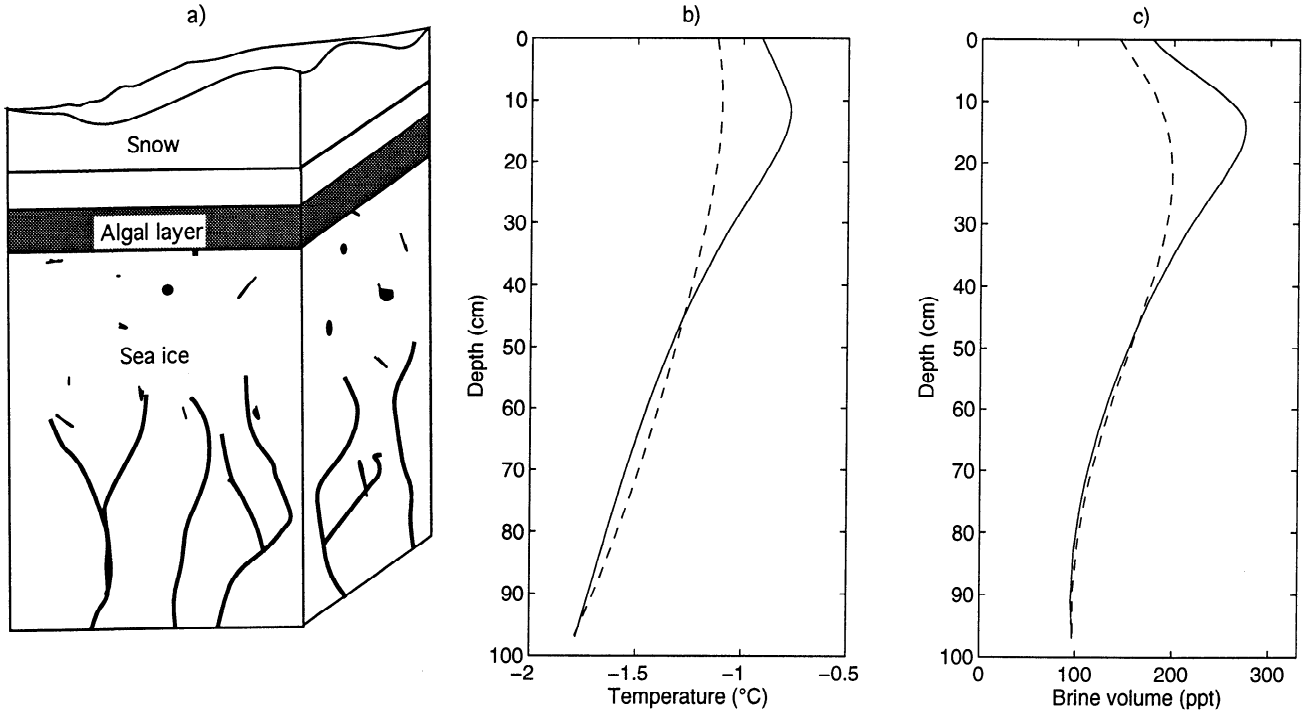

Figure 13. (a) Illustration of model configuration for high surface biomass concentrations. (b) Temperature profile on December 23 for algal free ice (dashed line) and for ice containing 250 mg chl a m^{-2} (solid line). The difference in sea ice temperature at a depth of 12 cm is 0.33 K. The snow depth is 5 cm. (c) Brine volume corresponding to the temperature profile in Figure 13b. The maximum in brine volume for algal free ice is 199 ppt and for ice containing algae 274 ppt.

depends on sea ice salinity and temperature, enhanced brine volumes were calculated for the top of the ice sheet (Figure 13c). Maximum brine volumes amount to 199 ppt at a depth of 22 cm for the algal free ice and 274 ppt at a depth of 14 cm for the ice containing algae. The mean brine volume in the upper 50 cm of the ice was 181 ppt for the algal free ice and 219 ppt for ice containing an algal standing stock of 250 mg chl a m^{-2}, corresponding to a 21% increase in brine volume.

To assess the integral effect of varying biomass and snow depth on the thermal regime and the increase in brine volume on the sea ice cover, a series of experiments was carried out. The change in brine volume in the upper 50 cm of an ice sheet containing algal biomass (as illustrated in Figure 13a) was calculated with respect to the predicted brine volume in an algal free ice column. Snow depth varied between 2 and 80 cm; algal biomass varied between 0 and 500 mg chl a m^{-2}. Massive surface and subsurface melting occurred in model calculations for snow free ice in late December. Snow free ice results in increased penetration of shortwave radiation into the upper layers of the ice due to the smaller albedo and extinction coefficient of the ice in comparison to snow. Since the model is based on molecular heat transfer and processes such as convectional heat transfer may occur due to the magnified brine volume, a simulation of snow free ice is not presented.

The results of this model integration show that significant changes in the brine volume occur only for small snow depth and high chlorophyll concentrations (Figure 14). A more detailed description is presented in Figure 15. A considerable rise in brine volume (>20-30%), brought about by the algae, should be expected for snow depths less than 5 cm and algal standing stocks exceeding 150 mg chl a m^{-2}, indicating that high light intensities and large amounts of biomass are required to produce any significant increase in melt rates or in brine volume.

4. Discussion

The model results strongly support speculations [*Sullivan et al.*, 1983; *Cota and Horne*, 1989; *Eicken et al.*, 1991b; *Roesler and Iturriaga*, 1994] that high algal biomass in sea ice enhances ice melting and hastens the destruction of the microalgal habitat. Model simulations of conditions reported for McMurdo Sound showed that enhanced light absorption and its conversion to heat by microalgae increased the temperature gradient at the bottom of the ice sheet, resulting in an additional bottom melting of about 4 cm over a melt period of approximately 40 days. Although the additional melting is negligible for the mass balance of sea ice, it may affect biological processes below the ice and have significant ecological consequences. For example, it has been proposed that biomass released from the ice into the water column may serve as a seed population, initiating an algal bloom in the water column, or serve as a

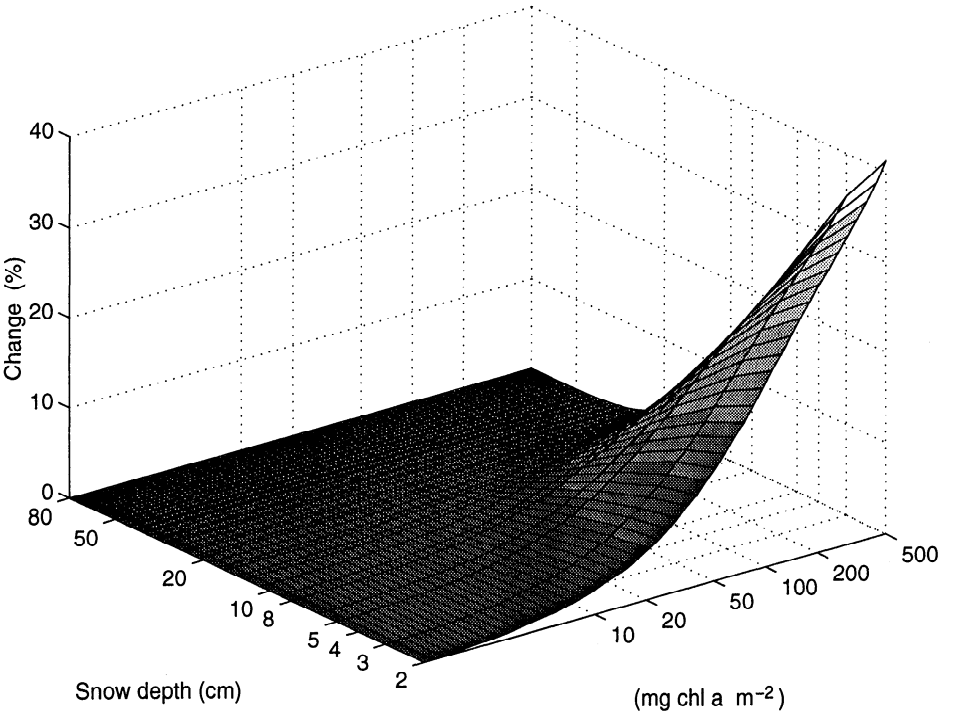

Figure 14. Calculated change in brine volume (in percent) as a function of snow depth and algal standing stock in the upper 50 cm of the ice. The model configuration is shown in Figure 13a. The thickness of the algal layer was 20 cm; the mean salinity was 4 ppt. The change in brine volume was calculated with regard to a model run for algal free ice and the corresponding snow depth.

food source for pelagic and benthic organisms (reviewed by *Legendre et al.* [1992]). Our results imply that the timing and time period over which the biomass release occurs would be regulated by the amount of biomass accumulation.

Light absorption in an ice free ocean occurs primarily in the upper tens to hundreds of meters and is usually dominated by light attenuation through seawater. Since algal biomass is distributed throughout a large volume of seawater, the chl *a* concentrations are comparatively

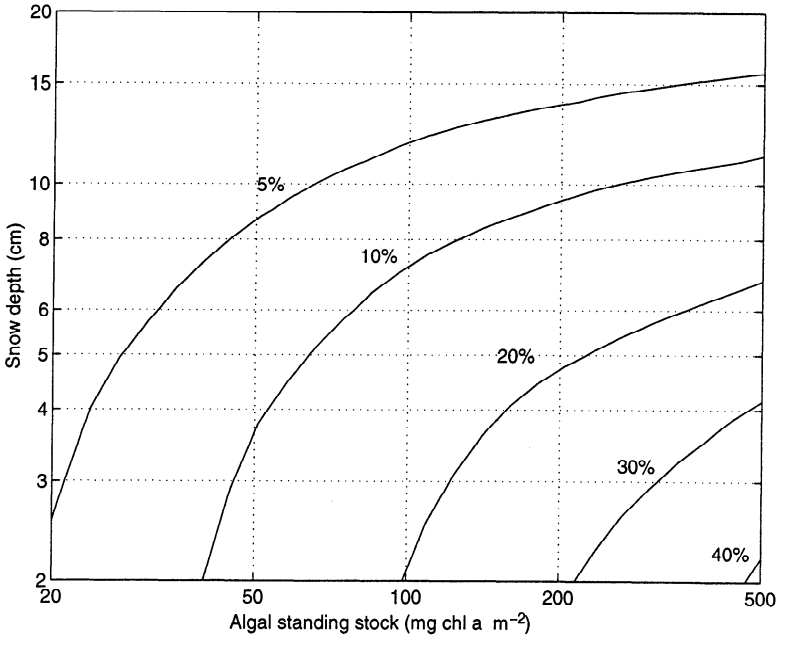

Figure 15. Changes in brine volume in the critical parameter range. A significant increase in brine volume (>20-30%) when algae are located at the top of the ice sheet may occur for snow depths less than 5 cm and algal standing stocks exceeding 150 mg chl *a* m^{-2}.

small. In contrast, sea ice contains high algal biomass concentrated within only a few meters. It is this vertical compression that makes light absorption by microalgae relevant for the heat budget of sea ice.

A set of model runs with high surface biomass concentration (see Figure 13a) indicated that localized heating from light absorption increases ice temperatures and, consequently, brine volume within the ice sheet. *Eicken et al.* [1991b] pointed out that porosity (i.e., brine volume) is a key variable in controlling ice strength. Compressive failure stresses anticorrelate with the total porosity of the ice [*Mellor*, 1986]. Thus sea ice microalgae could lower the ice strength by enhanced absorption of light and its conversion into heat. However, this effect only occurs when the algal standing stock is high (>150 mg chl a m^{-2}) and the snow load is small (<5 cm). The mean algal standing stocks observed in the Weddell Sea are 10-20 mg chl a m^{-2}, but local algal blooms may yield algal biomass that exceeds the critical value of 150 mg chl a m^{-2}. *Whitaker and Richardson* [1980] reported values up to 244 mg chl a m^{-2} observed in the sea ice at Signy Island, South Orkneys, Antarctica.

The brine volume (Figure 13c) was calculated from salinity and temperature profiles. The salinity profile (Figure 3) was obtained by fitting field data from *Eicken et al.* [1991a]. The mean salinity was about 4 ppt. Although this value is representative for the Weddell Sea, the evolution of such a salinity profile due to processes associated with brine expulsion or gravity drainage was excluded in the model. Since sea ice salinity exhibits high temporal and spatial variability, the calculated brine volume should be interpreted taking into account the limitations due to a static salinity profile which represents an average value inferred from field observations.

In areas where snow depth is small and biomass high, ice algae could influence the length and course of the ablation season. Under these conditions, decreased mechanical strength due to localized heating would hasten ice sheet breakup. Consequently, melting of the fragmented ice sheet would be enhanced, since heat from the surrounding water can be transferred more efficiently to smaller ice floe fragments [cf. *Maykut and Perovich*, 1987]. Increased brine volume also affects physical aspects of the habitat of sea ice organisms that may influence algal growth. Shape, volume, and extent of brine channels not only alter the penetration of light and rates of exchange of nutrients and gases, but also determine the amount of habitable space for organisms and the degree to which they are able to move or migrate within the ice [*Weissenberger et al.*, 1992]. Thus the increased brine volume caused by enhanced light absorption extends the sea ice habitat and enhances brine and nutrient fluxes.

5. Conclusions

By coupling a bio-optical model to a thermodynamic sea ice model, various results have been obtained to improve the understanding of biophysical interactions in sea ice. The proliferation of diatoms in the sea ice habitat and the resulting attenuation of light lead to a highly heterogeneous, vertical distribution of light in the ice column. The sea ice microalgae that are concentrated within a small layer (1-20 cm) at the bottom of the congelation ice in McMurdo Sound are predominantly diatoms, which produce photosynthetic pigments (chlorophyll a, chlorophyll c, and fucoxanthin) that strongly absorb light in the blue-green wavelengths. The majority of this absorbed light energy is converted into heat. By a validation of the bio-optical model we could affirm that, despite the simplifications of the bio-optical model, the results are consistent with field observations. Likewise, the spectral irradiance in sea ice, determined by the bio-optical model, is in accordance with model results from a more complicated four-stream model [*Grenfell*, 1991]. Thus the predicted light regime in sea ice could be used as a valid input for the thermodynamic model.

Microalgae may directly affect physical properties such as brine volume and can speed bottom melting by enhanced light absorption. The model integrations yielded magnified melt rates at the bottom of the ice sheet, implying that algae can increase the temperature gradient by absorption of shortwave radiation and its conversion into heat. As a consequence of the increased bottom melt rate, biomass may be released into the water column. The magnitude of melting is negligible for the energy and mass balance of the sea ice but may be of considerable ecological significance. Frequently, the timing and development of biological phenomena are determined by physical constraints. A remarkable result of this investigation is that the timing of bottom melting, a physical event, may be dominated by a biological process, at least under conditions typical for McMurdo Sound.

The results presented here should be assessed in the context of the simplifications made to develop the one-dimensional model. The complexity of biological and physical phenomena are reduced for the mathematical description. A one-stream model (Beer's law) is a poor approximation for thin ice [*Grenfell*, 1979] but sufficiently describes thick ice (>1 m). Doubtless, there are uncertainties in determining heat fluxes by using standard bulk aerodynamic formula. However, these approximations do not change the results essentially, since the difference in model results with and without including microalgae in the numerical scheme is the key result of the model integrations.

New features were included to determine additional heating and melting of sea ice through light absorption by microalgae. The calculation of the divergence of irradiance in every layer of the model provides the link between the thermodynamic model and the bio-optical model. In addition, photosynthesis is considered by an estimation of the photosynthetic efficiency, since a part of the absorbed energy is stored as photochemical energy and does not contribute directly to the heating of the ice.

Future applications of this model could include ab-

sorption of shortwave radiation by particulate inclusions, i.e., ice-rafted sediments in Arctic sea ice, or a more detailed study of the influence of microalgae on the length and course of the ablation season, thus furthering our understanding of radiative transfer and biophysical processes in sea ice.

Acknowledgments. The comments of three anonymous referees and suggestions by M. R. Lewis were of great value and are gratefully acknowledged. We also thank K. R. Arrigo for providing extinction coefficient data. Alfred-Wegener-Institut für Polar- und Meeresforschung publication 950.

References

Ackley, S. F., K. R. Buck, and S. Taguchi, Standing crop of algae in the sea ice of the Weddell Sea region, *Deep Sea Res., Part A, 26A,* 269-281, 1979.

Arrigo, K. R., C. W. Sullivan, and J. N. Kremer, A bio-optical model of Antarctic sea ice, *J. Geophys. Res., 96,* 10,581-10,592, 1991.

Arrigo, K. R., D. H. Robinson, and C. W. Sullivan, A high resolution study of the platelet ice ecosystem in McMurdo Sound, Antarctica: Photosynthetic and bio-optical characteristics of a dense microalgal bloom, *Mar. Ecol. Prog. Ser., 98,* 173-185, 1993.

Brine, D. T., and M. Iqbal, Diffuse and global solar spectral irradiance under cloudless skies, *Sol. Energy, 30,* 447-453, 1983.

Cota, G. F., and E. P. W. Horne, Physical control of Arctic ice algal production, *Mar. Ecol. Prog. Ser., 52,* 111-121, 1989.

Cox, G. F. N., and W. F. Weeks, Equations for determining the gas and brine volumes in sea-ice samples, *J. Glaciol., 29,* 306-316, 1983.

Cox, G. F. N., and W. F. Weeks, Numerical simulations of the profile properties of undeformed first-year sea ice during the growth season, *J. Geophys. Res., 93,* 12,449-12,460, 1988.

Crocker, G. B., and P. Wadhams, Modelling Antarctic fast-ice growth, *J. Glaciol., 35,* 3-8, 1989.

Dayton, P. K., G. A. Robilliard, and A. L. DeVries, Anchor ice formation in McMurdo Sound, Antarctica, and its biological effects, *Science, 163,* 273-274, 1969.

Dieckmann, G. S., K. Arrigo, and C. W. Sullivan, A high-resolution sampler for nutrient and chlorophyll *a* profiles of the sea ice platelet layer and underlying water column below fast ice in polar oceans: Preliminary results, *Mar. Ecol. Prog. Ser., 80,* 291-300, 1992.

Ebert, E. E., and J. A. Curry, An intermediate one-dimensional thermodynamic sea ice model for investigating ice-atmosphere interactions, *J. Geophys. Res., 98,* 10,085-10,109, 1993.

Eicken, H., Salinity profiles of Antarctic sea ice: Field data and model results, *J. Geophys. Res., 97,* 15,545-15,557, 1992.

Eicken, H., M. A. Lange, and G. S. Dieckmann, Spatial variability of sea-ice properties in the northwestern Weddell Sea, *J. Geophys. Res., 96,* 10,603-10,615, 1991a.

Eicken, H., S. F. Ackley, J. A. Richter-Menge, and M. A. Lange, Is the strength of sea ice related to its chlorophyll content?, *Polar Biol., 11,* 347-350, 1991b.

Grenfell, T. C., The effects of ice thickness on the exchange of solar radiation over the polar oceans, *J. Glaciol., 22,* 305-320, 1979.

Grenfell, T. C., A theoretical model of the optical properties of sea ice in the visible and near infrared, *J. Geophys. Res., 88,* 9723-9735, 1983.

Grenfell, T. C., A radiative transfer model for sea ice with vertical structure variations, *J. Geophys. Res., 96,* 16,991-17,001, 1991.

Grenfell, T. C., and G. A. Maykut, The optical properties of ice and snow in the Arctic Basin, *J. Glaciol., 18,* 445-463, 1977.

Grenfell, T. C., and D. K. Perovich, Spectral albedos of sea ice and incident solar irradiance in the southern Beaufort Sea, *J. Geophys. Res., 89,* 3573-3580, 1984.

Grossi, S. M., S. T. Kottmeier, R. L. Moe, G. T. Taylor, and C. W. Sullivan, Sea ice microbial communities, VI, Growth and primary production in bottom ice under graded snow cover, *Mar. Ecol. Prog. Ser., 35,* 153-164, 1987.

Horner, R., S. F. Ackley, G. S. Dieckmann, B. Gulliksen, T. Hoshiai, L. Legendre, I. A. Melnikov, W. S. Reeburgh, M. Spindler, and C. W. Sullivan, Ecology of sea ice biota, 1, Habitat, terminology, and methodology, *Polar Biol., 12,* 417-427, 1992.

Jeffries, M. O., W. F. Weeks, R. Shaw, and K. Morris, Structural characteristics of congelation and platelet ice and their role in the development of Antarctic land-fast sea ice, *J. Glaciol., 39,* 223-238, 1983.

Kipfstuhl, J., On the formation of underwater ice and the growth and energy budget of the sea ice in Atka Bay, Antarctica, (in German), *Ber. Polarforsch., 85,* 1991.

Kirk, J. T. O., *Light and Photosynthesis in Aquatic Ecosystems,* pp. 24-41, Cambridge Univ. Press, New York, 1983.

König-Langlo, G., The meteorological data of the Georg-von-Neumayer-Station (Antarctica) for 1988, 1989, 1990 and 1991, *Ber. Polarforsch., 116,* 1992.

Kottmeier, C., and R. Hartig, Winter observations of the atmosphere over Antarctic sea ice, *J. Geophys. Res., 95,* 16,551-16,560, 1990.

Leckner, B., The spectral distribution of solar radiation at the earth's surface - Elements of a model, *Sol. Energy, 20,* 143-150, 1978.

Legendre, L., S. F. Ackley, G. S. Dieckmann, B. Gulliksen, R. Horner, T. Hoshiai, I. A. Melnikov, W. S. Reeburgh, M. Spindler, and C. W. Sullivan, Ecology of sea ice biota, 2, Global significance, *Polar Biol., 12,* 429-444, 1992.

Leppäranta, M., and T. Manninen, The brine and gas content of sea ice with attention to low salinities and high temperatures, internal report, Finn. Inst. of Mar. Res., Helsinki, 1988.

Maykut, G. A., Energy exchange over young sea ice in the central Arctic, *J. Geophys. Res., 83,* 3646-3658, 1978.

Maykut, G. A., and T. C. Grenfell, The spectral distribution of light beneath first-year sea ice in the Arctic Ocean, *Limnol. Oceanogr., 20,* 554-563, 1975.

Maykut, G. A., and D. K. Perovich, The role of shortwave radiation in the summer decay of a sea ice cover, *J. Geophys. Res., 92,* 7032-7044, 1987.

Maykut, G. A., and N. Untersteiner, Some results from a time-dependent thermodynamic model of sea ice, *J. Geophys. Res., 76,* 1550-1575, 1971.

Mellor, M., Mechanical behavior of sea ice, in *The Geophysics of Sea Ice, NATO ASI Ser., Ser. B146,* edited by N. Untersteiner, pp. 165-281, Plenum, New York, 1986.

Morel, A., Available, usable, and stored radiant energy in relation to marine photosynthesis, *Deep Sea Res., 25,* 673-688, 1978.

Palmisano, A. C., and C. W. Sullivan, Sea ice microbial communities (SIMCO), 1, Distribution, abundance, and primary production of ice microalgae in McMurdo Sound, Antarctica in 1980, *Polar Biol., 2,* 171-177, 1983.

Palmisano, A. C., J. B. SooHoo, and C. W. Sullivan, Photosynthesis-irradiance relationships in sea ice microalgae from McMurdo Sound, Antarctica, *J. Phycol., 21,* 341-346, 1985.

Palmisano, A. C., M. P. Lizotte, G. A. Smith, P. D. Nichols, D. C. White, and C. W. Sullivan, Changes in photosynthetic carbon assimilation in Antarctic sea-ice diatoms during spring bloom: Variation in synthesis of lipid classes, *J. Exp. Mar. Biol. Ecol., 116,* 1-13, 1988.

Parkinson, C. L., and W. M. Washington, A large-scale numerical model of sea ice, *J. Geophys. Res., 84,* 311-337, 1979.

Perovich, D. K., G. F. Cota, G. A. Maykut, and T. C. Grenfell, Bio-optical observations of first-year Arctic sea ice, *Geophys. Res. Lett., 20,* 1059-1062, 1993.

Roesler, C. S., and R. Iturriaga, Absorption properties of marine-derived material in Arctic sea ice, *Proc. SPIE Int. Soc. Opt. Eng.,* vol. 2258, *Ocean Optics XII,* 933-943, 1994.

Schlosser, E., Optical studies of Antarctic sea ice, *Cold Reg. Sci. Technol., 15,* 289-293, 1988.

Schwerdtfeger, P., The thermal properties of sea ice, *J. Glaciol., 4,* 789-807, 1963.

Schwerdtfeger, W., The climate of the Antarctic, in *Climates of the Polar Regions, World Surv. of Climatol.,* vol. 14, edited by S. Orvig, pp. 253-356, Elsevier, Amsterdam, 1970.

Smith, R. E. H., W. G. Harrison, L. R. Harris, and A. W. Herman, Vertical fine structure of particulate matter and nutrients in sea ice of the high Arctic, *Can. J. Fish. Aquatic. Sci., 47,* 1348-1355, 1990.

SooHoo, J. B., A. C. Palmisano, S. T. Kottmeier, M. P. Lizotte, S. L. SooHoo, and C. W. Sullivan, Spectral light absorption and quantum yield of photosynthesis in sea ice microalgae and a bloom of *Phaeocystis pouchetii* from McMurdo Sound, Antarctica, *Mar. Ecol. Prog. Ser., 39,* 175-189, 1987.

Spencer, J. W., Fourier series representation of the position of the sun, *Search, 2,* 172, 1971.

Sullivan, C. W., A. C. Palmisano, S. T. Kottmeier, S. M. Grossi, R. Moe, and G. T. Taylor, The influence of light on development and growth of sea-ice microbial communities in McMurdo Sound, *Antarct. J. U.S., 18,* 100-102, 1983.

Thekaekara, M. P., Solar energy outside the earth's atmosphere, *Sol. Energy, 14,* 109-127, 1973.

van Loon, H., Cloudiness and precipitation in the southern hemisphere, in *Meteorology of the Southern Hemisphere,* edited by C. W. Newton, *Meteorol. Monogr., 13,* 101-111, 1972.

Weissenberger, J., G. S. Dieckmann, R. Gradinger, and M. Spindler, Sea ice: A cast technique to examine and analyze brine pockets and channel structure, *Limnol. Oceanogr., 37,* 179-183, 1992.

Whitaker, T. M., and M. G. Richardson, Morphology and chemical composition of a natural population of an ice-associated antarctic diatom *Navicula glaciei, J. Phycol., 16,* 250-257, 1980.

G. S. Dieckmann, H. Eicken, D. H. Robinson, D. Wolf-Gladrow, and R. E. Zeebe, Alfred-Wegener-Institut für Polar- und Meeresforschung, Postfach 12 01 61, D-27515 Bremerhaven, Germany. (e-mail: rzeebe@awi-bremerhaven.de)

(Received June 16, 1995; revised August 24, 1995; accepted August 25, 1995.)